ACS Photonics

pubs.acs.org/journal/apchd5

Article

Vibrational Hyper-Raman Molecular Spectroscopy with Entangled Photons

Feng Chen and Shaul Mukamel*

Cite This: https://doi.org/10.1021/acsphotonics.1c00777

Read Online

ACCESS | Metrics & More | Article Recommendations | Supporting Information

ABSTRACT: Time-energy entangled photons produced by spontaneous parametric down-conversion (SPDC) are employed to calculate vibrational hyper-Raman (HR) signals of the conjugated organic chromophore Wu112. Compared with classical light, time-energy entanglement can provide selectivity of Liouville-space pathways and thus suppress the strong broad electronic-Raman background arising from one-photon resonances of the intermediate states. The entangled-photon HR signal scales linearly with the SPDC pump field intensity rather than quadratically for classical light, which allows weak-field measurements on fragile samples.

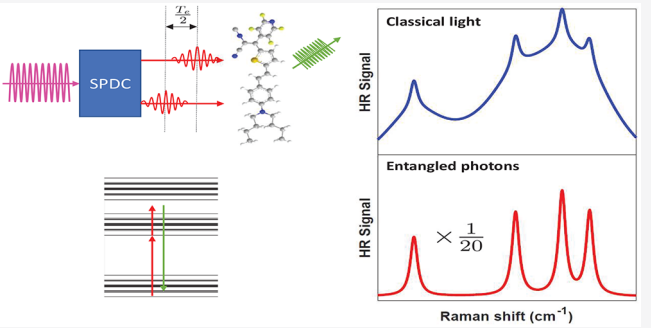

KEYWORDS: *entangled photons, hyper-Raman spectroscopy, Liouville-space pathways, one-photon resonances*

Entangled photons are of fundamental importance in quantum technologies such as computation,[1] communication,[2] and imaging.[3] Photons can be entangled in different degrees of freedom:[4−10] position, momentum, time, frequency, polarization, and orbital angular momentum. Growing efforts have been made recently to employ time-energy entangled photons in nonlinear molecular spectroscopy.[11−14] In entangled two-photon absorption,[15−30] the simultaneous temporal correlations and spectral anticorrelations can overcome Fourier-limitation on the joint temporal and spectral resolutions. Linear rather than quadratic scaling of signals with photon fluxes is another notable merit.

Here we focus on a different two-photon-induced signal: vibrational hyper-Raman scattering,[31] in which the absorption of two photons at frequencies ω_1 and ω_2 is accompanied by the spontaneous emission of a photon at frequency $\omega_r = \omega_1 + \omega_2 - \omega_{g'g}$, where $\omega_{g'g} = E_{g'} - E_g$ is a vibrational transition frequency at the ground electronic state manifold (see Figure 1b). This two-photon extension of linear Raman scattering has different selection rules so it can provide complementary information to infrared (IR) and Raman spectroscopy. For example, the HR signal can reveal "silent modes"[32] that are both IR and Raman inactive. It has also been shown that, in combination with linear Raman scattering, HR scattering can help disentangle overlapping electronic transitions in the absorption spectrum.[33,34]

Typically, HR signals are extremely weak (10^5−10^7 weaker than ordinary Raman signals). One way to enhance the signals is through electronic resonances.[35] Hitherto, most studies have focused on two-photon resonant HR signals, but the two-photon-induced fluorescence can severely erode the signal-to-noise ratio of the HR spectrum. Here, we study HR signals of a conjugated organic chromophore Wu112 with one-photon but no two-photon resonances, thus, avoiding the fluorescence background. We find that classical HR signals are greatly enhanced by the one-photon resonances of the intermediate states, but this enhancement is accompanied by a strong broad electronic-Raman background, which can dominate the sharp HR peaks. However, by applying time-energy entangled photons produced by type-I SPDC,[4,11] we show that the Liouville-space pathways contributing to this background can be suppressed. Moreover, rather than quadratic scaling with the pump field intensity in the classical case, the entangled-photon HR signal scales linearly with the pump field intensity and thus enables HR measurements on fragile samples at low photon fluxes. In the Supporting Information we also examine the HR signals with a two-photon, but no one-photon resonance, and find that entangled photons have no effect on the relative intensities of the fluorescence and HR components, but simply scale both equally.

This paper is structured as follows: We first introduce the vibronic Hamiltonian for Wu112. We next present the expression for the HR signal. Then, we calculate the HR signals generated by classical light both resonant and off-resonant with the intermediate electronic state and discuss the

Received: May 26, 2021

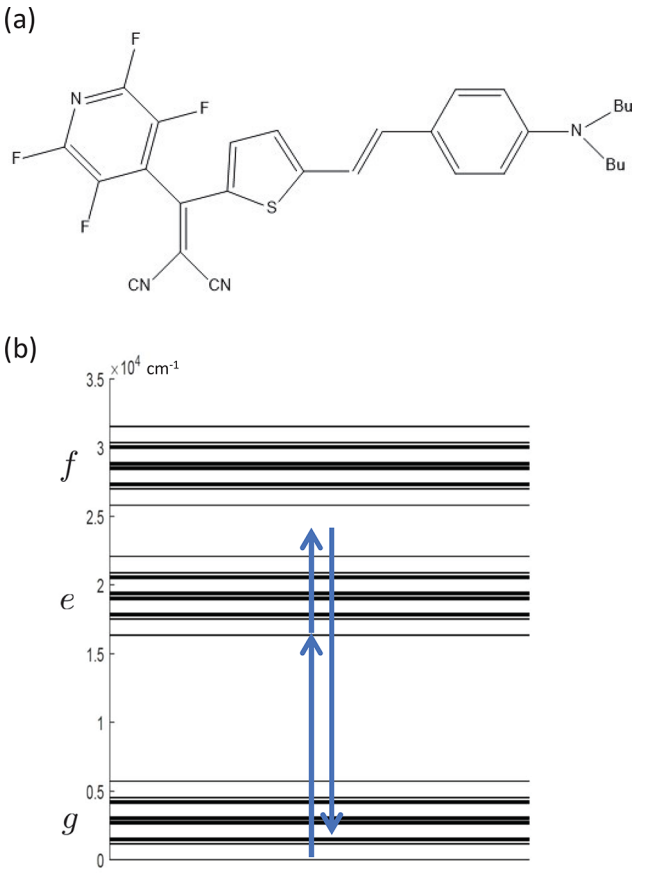

Figure 1. Molecular structure (a) and level scheme (b) of Wu112. It is described by a vibronic model in eq 1 with parameters $E_g = 0$, $E_e = 16350\ \mathrm{cm}^{-1}$, $E_f = 25800\ \mathrm{cm}^{-1}$, $\omega_1 = 1184\ \mathrm{cm}^{-1}$, $\omega_2 = 1420\ \mathrm{cm}^{-1}$, $\omega_3 = 1528\ \mathrm{cm}^{-1}$, $\omega_4 = 1592\ \mathrm{cm}^{-1}$, $\lambda_{e1} = 767\ \mathrm{cm}^{-1}$, $\lambda_{e2} = 953\ \mathrm{cm}^{-1}$, $\lambda_{e3} = 1081\ \mathrm{cm}^{-1}$, $\lambda_{e4} = 981\ \mathrm{cm}^{-1}$, $\lambda_{f1} = 940\ \mathrm{cm}^{-1}$, $\lambda_{f2} = 1167\ \mathrm{cm}^{-1}$, $\lambda_{f3} = 1323\ \mathrm{cm}^{-1}$, and $\lambda_{f4} = 1202\ \mathrm{cm}^{-1}$.

signal enhancement and the strong broad background. Finally, we introduce the entangled-photon state and demonstrate the suppression of this background by time-energy entanglement.

THE VIBRONIC MODEL

The thiophene derivative Wu112 (see Figure 1) is a "push–pull" conjugated system with a strong intermolecular charge transfer band around 600 nm in cyclohexane.[36] It is described by the following vibronic Hamiltonian:

$$H_M = \sum_{s=g,e,f} E_s|s\rangle\langle s| + \sum_{\mu=1}^{4} \omega_\mu a_\mu^\dagger a_\mu + \sum_{s=e,f}\sum_{\mu} \lambda_{s\mu}|s\rangle\langle s|(a_\mu^\dagger + a_\mu + \lambda_{s\mu}/\omega_\mu) \tag{1}$$

where the three terms represent the electronic and vibrational degrees of freedom and their couplings, respectively; a_μ and $a_\mu^\dagger$ are the annihilation and creation operators of the μ-th vibrational mode; $\lambda_{s\mu}$ is the coupling strength between electronic state s and vibrational mode μ. The model has three electronic states (ground state g, intermediate state e, and doubly excited state f) and the four dominant vibrational modes in the HR spectra reported in ref 36.

We assume a dipole light–matter interaction Hamiltonian in the rotating wave approximation,

$$H_I = -V^\dagger \sum_{j=1,2,r} \hat{E}_j(t) + \mathrm{H.c.} \tag{2}$$

where V and $V^\dagger$ are the lowering and raising parts of the transition dipole operators. $\hat{E}_j = \int_0^\infty \mathrm{d}\omega_j \sqrt{\frac{\hbar\bar{\omega}_j}{4\pi\epsilon_0 cA}}\, a_j(\omega_j) e^{-i\omega_j t}$ is the positive-frequency component of the electric field operator of the first/second/emitted ($j = 1, 2, r$) photon beam, where a_j and $a_j^\dagger$ are the annihilation and creation operators for beam j photons that satisfy $[a(\omega), a^\dagger(\omega')] = \delta(\omega - \omega')$, c is the light velocity, A is the effective area of the field, and the slowly varying envelope approximation has been applied, which assumes that the field bandwidths are negligible compared to the central frequencies $\bar{\omega}_j$.[37]

HYPER-RAMAN SIGNAL

The HR signal is defined as the emission rate of photons with frequency ω_r:

$$S(\omega_r) = \lim_{t\to\infty} \frac{\mathrm{d}}{\mathrm{d}t}\langle a_r^\dagger a_r\rangle \tag{3}$$

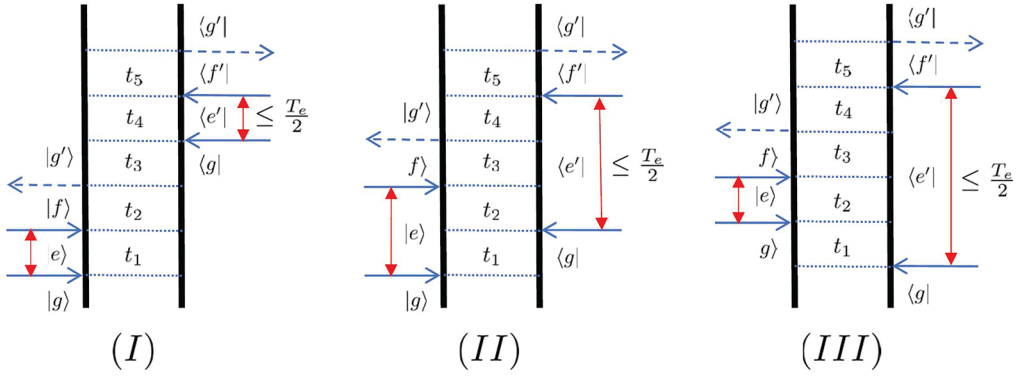

Figure 2. Ladder diagrams representing the Liouville-space pathways of HR signals for systems with two-photon off-resonant doubly excited states. Their complex conjugates are given by other diagrams (not shown). Incoming arrows denote photon absorptions and outgoing arrows denote photon emissions. On each side, two photon absorptions are followed by one photon emission. When the entangled photons are employed, the time interval between two photon absorptions on each side is limited by the entanglement time T_e (see the red arrows). In diagram (II), no event happens on the ket side within the time interval between the two photon absorptions on the bra side. In contrast, there are one absorption and one emission events on the ket side within the corresponding time interval in diagram (II) and two absorption and one emission events for diagram (III). Therefore, diagrams (II) and (III) are suppressed for sufficiently short T_e.

https://doi.org/10.1021/acsphotonics.1c00777
ACS Photonics XXXX, XXX, XXX−XXX

To the sixth order in the light−matter interaction, and considering that the f states are far off-resonant from the two-photon frequency, we find that six Liouville-space pathways contribute to the signal (given by diagrams in Figure 2 and their complex conjugate pairs; for diagram rules, see ref 38). They give

$$
\begin{aligned}
&S(\omega_r) = 2\mathrm{Re}(S_I + S_{II} + S_{III})\\
&S_I = \sum_{g'ee'ff'} \int_0^\infty \mathrm{d}t_{1\sim5} G^{(2)}(t_1 + t_2 + t_3 + t_4, t_1 + t_2 + t_3, t_1, 0)\\
&\times e^{-(i\omega_{eg}+\gamma_{eg})t_1-(i\omega_{fg}+\gamma_{fg})t_2-(i\omega_r+i\omega_{g'g}+\gamma_{g'g})t_3-(i\omega_r-i\omega_{e'g'}+\gamma_{eg})t_4}\\
&\times e^{-i(\omega_r-\omega_{f'g'}-i\gamma_{fg})t_5} C_{geff'e'g'}\\
&S_{II} = \sum_{g'ee'ff'} \int_0^\infty \mathrm{d}t_{1\sim5} G^{(2)}(t_1, t_1 + t_2 + t_3 + t_4, t_1 + t_2, 0)\\
&\times e^{-i(\omega_{eg}-i\gamma_{eg})t_1-i(\omega_{ee'}-i\gamma_{ee'})t_2-i(\omega_{fe'}-i\gamma_{fe'})t_3-i(\omega_r-\omega_{e'g'}-i\gamma_{eg})t_4}\\
&\times e^{-i(\omega_r-\omega_{f'g'}-i\gamma_{fg})t_5} C_{geff'e'g'}\\
&S_{III} = \sum_{g'ee'ff'} \int_0^\infty \mathrm{d}t_{1\sim5} G^{(2)}(0, t_1 + t_2 + t_3 + t_4, t_1 + t_2, t_1)\\
&\times e^{i(\omega_{e'g}+i\gamma_{eg})t_1+i(\omega_{ee'}+i\gamma_{ee'})t_2-i(\omega_{fe'}-i\gamma_{fe'})t_3-i(\omega_r-\omega_{e'g'}-i\gamma_{eg})t_4}\\
&\times e^{-i(\omega_r-\omega_{f'g'}-i\gamma_{fg})t_5} C_{geff'e'g'}
\end{aligned}
\tag{4}
$$

where $C_{geff'e'g'} = V_{ge'}V_{e'f'}V^*_{g'f'}V_{g'f}V^*_{ef}V^*_{ge}$, $G^{(2)}(t_a, t_b, t_c, t_d) = \langle E^\dagger(t_a)E^\dagger(t_b)E(t_c)E(t_d)\rangle$ is the field correlation function in the interaction picture, and γs are the electronic and vibrational dephasing rates. S_I, S_{II}, and S_{III} correspond to diagrams (I), (II), and (III) in Figure 2, respectively. The field correlation function $G^{(2)}$ depends on the nature of the light source.

Classical Light. In the following, we use two classical monochromatic pump pulses with frequencies ω_1 and ω_2 to excite the molecule. The difference between ω_1 and ω_2 is much larger than the vibrational frequency, so we can focus on two-photon excitation induced by one photon from each pulse, because signals induced by two photons from the same pulse will be in different frequency regimes. Additionally, two-photon excitation energy $\omega_1 + \omega_2$ lies in the gap between the e and f vibronic manifold to avoid two-photon resonances. With $E_{1,2}(t) = \alpha_P L(\omega_{1,2})e^{-i\omega_{1,2}t}$, where $L(\omega_{1,2}) = \sqrt{\frac{\hbar\omega_{1,2}}{4\pi\epsilon_0 cA}}$ and $|\alpha_P|^2$ defines the pump photon flux, we obtain

$$
\begin{aligned}
\langle E^\dagger(t_d)E^\dagger(t_c)E(t_b)E(t_a)\rangle &= \sum_{i,j=1,2} E^*_j(t_d)E^*_j(t_c)E_{\bar{i}}(t_b)E_i(t_a)\\
&= |\alpha_P|^4 L(\omega_1)^2 L(\omega_2)^2 \sum_{i,j=1,2} e^{i(\omega_{\bar{j}}t_d+\omega_j t_c-\omega_{\bar{i}}t_b-\omega_i t_a)}
\end{aligned}
\tag{5}
$$

where $\bar{i} = 3 - i$ and $\bar{j} = 3 - j$. Substituting the above expression into eq 4, we obtain

$$
\begin{aligned}
&S_I(\omega_r) = |\alpha_P|^4 L(\omega_1)^2 L(\omega_2)^2 \sum_{i,j=1,2}\sum_{g'ee'ff'} \frac{C_{geff'e'g'}}{(\omega_1 + \omega_2 - \omega_{fg} + i\gamma_{fg})(\omega_r - \omega_{f'g'} - i\gamma_{fg})}\\
&\times \frac{1}{(\omega_i - \omega_{eg} + i\gamma_{eg})(\omega_r - \omega_{e'g'} - \omega_j - i\gamma_{eg})}\\
&\times \frac{\gamma_{g'g}}{(\omega_1 + \omega_2 - \omega_r - \omega_{g'g})^2 + \gamma^2_{g'g}}\\
&S_{II}(\omega_r) = |\alpha_P|^4 L(\omega_1)^2 L(\omega_2)^2 \sum_{i,j=1,2}\sum_{g'ee'ff'} \frac{C_{geff'e'g'}}{(\omega_r - \omega_{f'g'} - i\gamma_{fg})(\omega_i - \omega_{eg} + i\gamma_{eg})}\\
&\times \frac{1}{(\omega_j - \omega_{fe'} + i\gamma_{fe'})(\omega_i - \omega_{\bar{j}} + \omega_{ee'} - i\gamma_{ee'})}\\
&\times \frac{\gamma_{eg}}{(\omega_r - \omega_{eg} - \omega_j)^2 + \gamma^2_{eg}}\\
&S_{III}(\omega_r) = |\alpha_P|^4 L(\omega_1)^2 L(\omega_2)^2 \sum_{i,j=1,2}\sum_{g'ee'ff'} \frac{C_{geff'e'g'}}{(\omega_r - \omega_{f'g'} - i\gamma_{fg})(\omega_{\bar{j}} - \omega_{e'g} - i\gamma_{e'g})}\\
&\times \frac{1}{(\omega_j - \omega_{fe'} + i\gamma_{fe'})(\omega_i - \omega_{\bar{j}} + \omega_{e'e} + i\gamma_{e'e})}\\
&\times \frac{\gamma_{eg}}{(\omega_r - \omega_{e'g'} - \omega_j)^2 + \gamma^2_{eg}},
\end{aligned}
\tag{6}
$$

where the last term in S_I is obtained by dropping the real part of $1/(\omega_1 + \omega_2 - \omega_{g'g} + i\gamma_{g'g})$ because it gives unphysical fluorescence even when f states are far off-resonant.[38] S_{II} and S_{III} were obtained similarly.

Resonant Pump. We first assume that the pulse 1 is resonant with the intermediate states, that is, $\omega_1 \approx \omega_{eg}$. We note a key difference between diagrams (I) and (II-III). The latter two can be seen as a one-photon absorption to an e state followed by an electronic Raman scattering from e to g' through virtual states f. Hence, the emitted light should have resonances at $\omega_r = \omega_2 + \omega_{eg'} \approx \omega_1 + \omega_2 - \omega_{g'g}$, with a broad line width characterized by the electronic dephasing rate γ_{eg}, as shown in the last Lorentzian terms of S_{II} and S_{III} in eq 6. In contrast, there is no e-state population ($|e\rangle\langle e|$) throughout diagram (I). It has resonances at $\omega_r = \omega_1 + \omega_2 - \omega_{g'g}$ but with a much narrower bandwidth characterized by a ground-state slow vibrational dephasing rate $\gamma_{g'g}$. Thus, the total signal contains narrow peaks on top of the broad electronic-Raman background. This background makes it hard to observe the narrow HR peaks, as shown in Figure 3a. The high spectral resolution of diagram (I) is lowered due to a strong broad background from diagrams (II) and (III).

Off-Resonant Pump. If both pulses are electronically off-resonant, the relative contributions from diagrams (II) and (III) are reduced due to the occupation of the e states, and thus, diagram (I) will dominate and its spectral resolution is retained. The trade-off is that the off-resonant signal intensity is significantly reduced, as is seen in Figure 3b.

Time-Energy Entangled Photons. We now turn to the central result of this paper: suppresion of the strong electronic-Raman background in classical one-photon resonant HR signals by time-energy entangled photons. Entangled photons generated via type-II SPDC pumped by a monochromatic laser of frequency ω_P are described by the two-photon state:[4,11]

$$
|\Psi\rangle = \iint \mathrm{d}\omega_i \mathrm{d}\omega_s \phi(\omega_i, \omega_s) a^\dagger_i(\omega_i) a^\dagger_s(\omega_s)|\Omega\rangle \tag{7}
$$

https://doi.org/10.1021/acsphotonics.1c00777
ACS Photonics XXXX, XXX, XXX−XXX

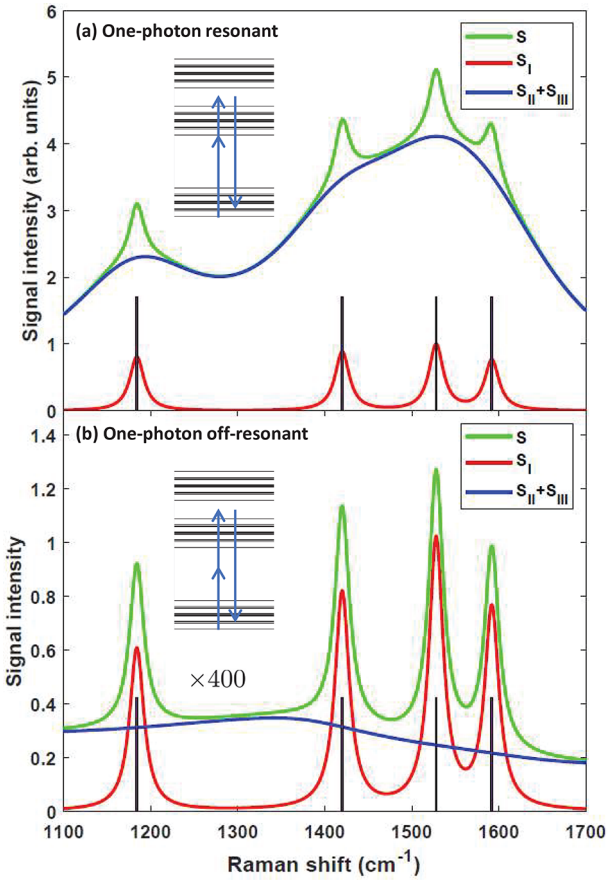

Figure 3. Classical HR signals: resonant vs off-resonant. *X*-axis is the Raman shift $\omega_1 + \omega_2 - \omega_r$. Vibrational transitions are marked by vertical bars. The insets are the excitation pathways. (a) One-photon resonant pump: ω_1 = 16350 cm^{-1} and ω_2 = 7179 cm^{-1}. Narrow spectral features of diagram (I) are dominated by the strong broad background given by diagrams (II) and (III); (b) Off-resonant pump: ω_1 = 12000 cm^{-1} and ω_2 = 11529 cm^{-1}. Diagram (I) dominates the signal, and thus, high spectral resolution is retained. But the signal intensity is much weaker than that of the resonant case. Both plots use the same units, and the signal in (b) is magnified by 400×, which is chosen such that the maximum of S_I component is around 1. Pump photon flux is $|\alpha_P|^2 = 10^{10}$/s and dephasing parameters are $\gamma_{ee'} = \gamma_{gg'} = \gamma_{ff'} = 10$ cm^{-1}, $\gamma_{fe} = 400$ cm^{-1}, $\gamma_{fg} = 600$ cm^{-1}, and $\gamma_{eg} = 100$ cm^{-1}.

with the two-photon envelope

$$\phi(\omega_i, \omega_s) = \alpha_P \sqrt{\frac{T_e}{4\pi}}\, \delta(\omega_i + \omega_s - \omega_P)\mathrm{sinc}((\omega_i - \bar{\omega}_i)T_e/2) \tag{8}$$

Here $a_i^\dagger$ and $a_s^\dagger$ are the creation operators for the idler and signal modes respectively, T_e is the entanglement time, ω_P is the monochromatic pump frequency and is chosen to lie in the gap between the e and f vibronic manifold, $\bar{\omega}_i$ is central frequency of the idler photon and is taken to be resonant with the electronic excitation, $\bar{\omega}_s$ is the central frequency of the signal photon, and the Dirac delta function is responsible for the frequency anticorrelation: $\omega_i + \omega_s = \omega_P$. We thus get,[4,11]

$$\langle \Psi | E^\dagger(t_d) E^\dagger(t_c) E(t_b) E(t_a) | \Psi \rangle = \frac{\pi |\alpha_P|^2}{T_e} L(\bar{\omega}_i)^2 L(\bar{\omega}_s)^2 \times \sum_{\mathbf{p}} e^{i(\bar{\omega}_{p_4} t_d + \bar{\omega}_{p_3} t_c - \bar{\omega}_{p_2} t_b - \bar{\omega}_{p_1} t_a)} \Pi\left(\frac{t_d - t_c}{T_e}\right) \Pi\left(\frac{t_b - t_a}{T_e}\right) \tag{9}$$

The subscript $\boldsymbol{p} = \{p_1, p_2, p_3, p_4\}$ labels the beams (i or s) that interact with the molecule at times $\{t_a, t_b, t_c, t_d\}$, and $\Pi(\cdot)$ is the rectangular function: $\Pi(x) = 1/2$ for $-1/2 < x < 1/2$ and 0 otherwise. The rectangular functions guarantee that two photons arrive together within $T_e/2$. Substituting the above expression into eq 4, we obtain

$$S_I(\omega_r) = \frac{\pi |\alpha_P|^2}{T_e} L(\bar{\omega}_i)^2 L(\bar{\omega}_s)^2 \sum_{g'ee'ff'} \sum_{\mathbf{p}} \frac{C_{geff'e'g'}}{\omega_P - \omega_{fg} + i\gamma_{fg}} \times \frac{1}{\omega_r - \omega_{f'g'} - i\gamma_{fg}} \frac{e^{i(\bar{\omega}_{\mathbf{p}_1} - \omega_{eg} + i\gamma_{eg})T_e/2} - 1}{i(\bar{\omega}_{\mathbf{p}_1} - \omega_{eg} + i\gamma_{eg})} \times \frac{e^{i(\bar{\omega}_{\mathbf{p}_4} + \omega_{eg} - \omega_r + i\gamma_{eg})T_e/2} - 1}{i(\bar{\omega}_{\mathbf{p}_4} + \omega_{e'g'} - \omega_r + i\gamma_{eg})} \times \frac{\gamma_{g'g}}{(\omega_P - \omega_r - \omega_{g'g})^2 + \gamma_{g'g}^2} \tag{10}$$

S_{II} and S_{III} are given in the Supporting Information.

In diagrams (II) and (III) of Figure 2, there is at least one absorption and one emission event on the ket side within the time interval between two photon absorptions on the bra. In contrast, there is no event within the corresponding time interval in diagram (I). For a short entanglement time, the idler and signal photons are absorbed almost simultaneously, and it is unlikely that additional events can happen in between. From eq 4 (see Supporting Information), we can show that $S_{II,III}/S_I \sim O(T_e)$ as $T_e \to 0$, so $S_I \gg S_{II} + S_{III}$ for short enough T_e.

As shown in the upper panel of Figure 4c, S_I is the dominant contribution to the total HR signal at T_e = 50 fs. S_I is sharply peaked at the vibrational transitions with line width characterized by the vibrational dephasing rate $\gamma_{gg'}$, as can be seen from the last Lorentzian term in eq 10. As the entanglement time is increased, the aforementioned restriction is relaxed, so the relative contributions from diagrams (II) and (III) should become stronger, as verified in the lower panel of Figure 4c for T_e = 1 ps. Thus, entangled photons with a sufficiently short entanglement time can suppress the electronic-Raman background from diagrams (II) and (III).

We further note that eq 10 scales linearly with the pump intensity $|\alpha_P|^2$, in contrast with the quadratic scaling in the classical case, eq 6. The entangled-photon HR signals are therefore stronger than the classical ones at low pump intensities, as shown in Figure 4c for $|\alpha_P|^2 = 10^{10}$/s.

CONCLUSIONS

We have shown that one-photon resonances can significantly enhance the classical HR signals, but they also introduce a strong broad electronic-Raman background. By pathway selectivity, time-energy entangled photons can suppress this background while retaining the intense and narrow hyper-Raman peaks. Another advantage of entangled light for HR

https://doi.org/10.1021/acsphotonics.1c00777
ACS Photonics XXXX, XXX, XXX−XXX

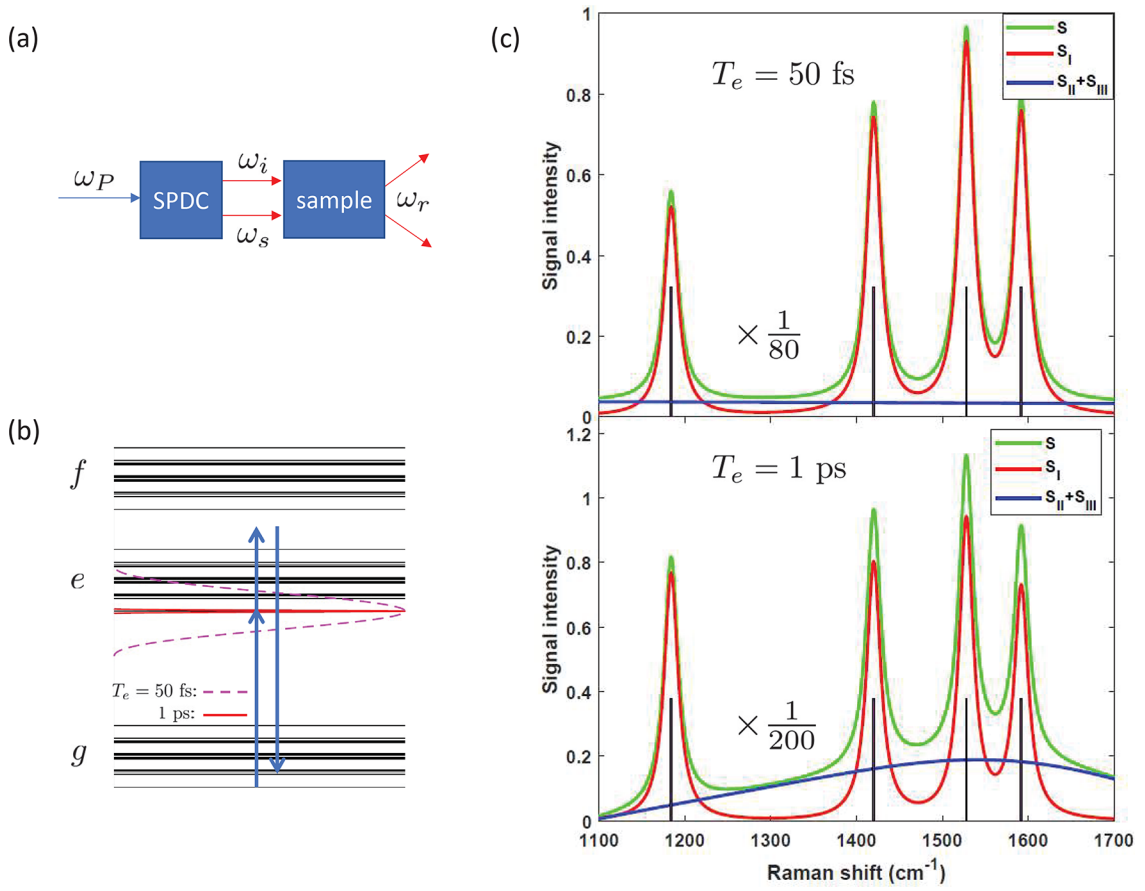

Figure 4. (a) Schematic of the hyper-Raman spectroscopy with entangled photons generated by SPDC; (b) Transition pathway. The intermediate state is one-photon resonant, and the bandwidth of single photons is characterized by $2\pi/T_e$ (see the envelopes); (c) HR signals with entangled photons: T_e = 50 fs vs T_e = 1 ps. Upper panel: T_e = 50 fs. Total signal is sharply peaked at the vibrational transitions marked by vertical bars. As explained in the main text, $S_I \gg S_{II} + S_{III}$; Lower panel: T_e = 1 ps. The relative contributions from S_{II} and S_{III} become stronger when T_e is increased. Compared with classical signals in Figure 3, entangled-photon signals are enhanced due to its linear scaling with pump intensity. Here, ω_P = 23529 cm^{-1}, $\bar{\omega}_s$ = 16350 cm^{-1}, and $\bar{\omega}_i$ = 7179 cm^{-1}. Signal intensity scales, pump photon fluxes, and dephasing parameters are the same as those in Figure 3.

spectroscopy is that the signal scales linearly with the pump intensity rather than quadratically. At low field intensities, entangled photons give stronger signals than classical light and therefore are useful for experiments on fragile biological samples.

■ ASSOCIATED CONTENT

Supporting Information

The Supporting Information is available free of charge at https://pubs.acs.org/doi/10.1021/acsphotonics.1c00777.

S1: Expressions for S_{II} and S_{III} with entangled photons; S2: Fluorescence and hyper-Raman signals with classical light and entangled photons for one-photon off-resonant but two-photon resonant experimental setting (PDF)

■ AUTHOR INFORMATION

Corresponding Author

Shaul Mukamel − *Department of Chemistry and Department of Physics and Astronomy, University of California, Irvine, California 92697, United States;* orcid.org/0000-0002-6015-3135; Email: smukamel@uci.edu

Author

Feng Chen − *Department of Chemistry and Department of Physics and Astronomy, University of California, Irvine, California 92697, United States*

Complete contact information is available at: https://pubs.acs.org/10.1021/acsphotonics.1c00777

Notes

The authors declare no competing financial interest.

■ ACKNOWLEDGMENTS

This work was primarily supported by the U.S. Department of Energy, Office of Science, Office of Basic Energy Sciences under Award DE-SC0020168 (S.M). The support of NSF Grant CHE-1953045 is gratefully acknowledged.

■ REFERENCES

(1) Slussarenko, S.; Pryde, G. J. Photonic quantum information processing: A concise review. *Appl. Phys. Rev.* **2019**, *6*, 041303.
(2) Gisin, N.; Ribordy, G.; Tittel, W.; Zbinden, H. Quantum cryptography. *Rev. Mod. Phys.* **2002**, *74*, 145−195.
(3) Moreau, P.-A.; Toninelli, E.; Gregory, T.; Padgett, M. J. Imaging with quantum states of light. *Nat. Rev. Phys.* **2019**, *1*, 367−380.

(4) Keller, T. E.; Rubin, M. H. Theory of two-photon entanglement for spontaneous parametric down-conversion driven by a narrow pump pulse. *Phys. Rev. A: At., Mol., Opt. Phys.* **1997**, *56*, 1534−1541.
(5) Brendel, J.; Gisin, N.; Tittel, W.; Zbinden, H. Pulsed Energy-Time Entangled Twin-Photon Source for Quantum Communication. *Phys. Rev. Lett.* **1999**, *82*, 2594−2597.
(6) Nambu, Y.; Usami, K.; Tsuda, Y.; Matsumoto, K.; Nakamura, K. Generation of polarization-entangled photon pairs in a cascade of two type-I crystals pumped by femtosecond pulses. *Phys. Rev. A: At., Mol., Opt. Phys.* **2002**, *66*, 033816.
(7) Edamatsu, K.; Oohata, G.; Shimizu, R.; Itoh, T. Generation of ultraviolet entangled photons in a semiconductor. *Nature* **2004**, *431*, 167−170.
(8) Akopian, N.; Lindner, N. H.; Poem, E.; Berlatzky, Y.; Avron, J.; Gershoni, D.; Gerardot, B. D.; Petroff, P. M. Entangled Photon Pairs from Semiconductor Quantum Dots. *Phys. Rev. Lett.* **2006**, *96*, 130501.
(9) Fickler, R.; Campbell, G.; Buchler, B.; Lam, P. K.; Zeilinger, A. Quantum entanglement of angular momentum states with quantum numbers up to 10,010. *Proc. Natl. Acad. Sci. U. S. A.* **2016**, *113*, 13642−13647.
(10) Howell, J. C.; Bennink, R. S.; Bentley, S. J.; Boyd, R. W. Realization of the Einstein-Podolsky-Rosen Paradox Using Momentum- and Position-Entangled Photons from Spontaneous Parametric Down Conversion. *Phys. Rev. Lett.* **2004**, *92*, 210403.
(11) Dorfman, K. E.; Schlawin, F.; Mukamel, S. Nonlinear optical signals and spectroscopy with quantum light. *Rev. Mod. Phys.* **2016**, *88*, 045008.
(12) Mukamel, S.; et al. Roadmap on quantum light spectroscopy. *J. Phys. B: At., Mol. Opt. Phys.* **2020**, *53*, 072002.
(13) Szoke, S.; Liu, H.; Hickam, B. P.; He, M.; Cushing, S. K. Entangled light−matter interactions and spectroscopy. *J. Mater. Chem. C* **2020**, *8*, 10732−10741.
(14) Schlawin, F. Entangled photon spectroscopy. *J. Phys. B: At., Mol. Opt. Phys.* **2017**, *50*, 203001.
(15) Saleh, B. E. A.; Jost, B. M.; Fei, H.-B.; Teich, M. C. Entangled-Photon Virtual-State Spectroscopy. *Phys. Rev. Lett.* **1998**, *80*, 3483−3486.
(16) Peřina, J.; Saleh, B. E. A.; Teich, M. C. Multiphoton absorption cross section and virtual-state spectroscopy for the entangled *n*-photon state. *Phys. Rev. A: At., Mol., Opt. Phys.* **1998**, *57*, 3972−3986.
(17) de J León-Montiel, R.; Svozilík, J.; Salazar-Serrano, L. J.; Torres, J. P. Role of the spectral shape of quantum correlations in two-photon virtual-state spectroscopy. *New J. Phys.* **2013**, *15*, 053023.
(18) Oka, H. Efficient selective two-photon excitation by tailored quantum-correlated photons. *Phys. Rev. A: At., Mol., Opt. Phys.* **2010**, *81*, 063819.
(19) Schlawin, F.; Dorfman, K. E.; Mukamel, S. Entangled Two-Photon Absorption Spectroscopy. *Acc. Chem. Res.* **2018**, *51*, 2207−2214.
(20) Howell, J. C.; Bennink, R. S.; Bentley, S. J.; Boyd, R. W. Realization of the Einstein-Podolsky-Rosen Paradox Using Momentum- and Position-Entangled Photons from Spontaneous Parametric Down Conversion. *Phys. Rev. Lett.* **2004**, *92*, 210403.
(21) Lee, D.-I.; Goodson, T. Entangled photon absorption in an organic porphyrin dendrimer. *J. Phys. Chem. B* **2006**, *110*, 25582−25585.
(22) Schlawin, F.; Dorfman, K. E.; Fingerhut, B. P.; Mukamel, S. Suppression of population transport and control of exciton distributions by entangled photons. *Nat. Commun.* **2013**, *4*, 1−7.
(23) Guzman, A. R.; Harpham, M. R.; Süzer, O.; Haley, M. M.; Goodson, T. G. Spatial Control of Entangled Two-Photon Absorption with Organic Chromophores. *J. Am. Chem. Soc.* **2010**, *132*, 7840−7841.
(24) Kang, G.; Nasiri Avanaki, K.; Mosquera, M. A.; Burdick, R. K.; Villabona-Monsalve, J. P.; Goodson, T., III; Schatz, G. C. Efficient Modeling of Organic Chromophores for Entangled Two-Photon Absorption. *J. Am. Chem. Soc.* **2020**, *142*, 10446−10458.
(25) Varnavski, O.; Pinsky, B.; Goodson, T. Entangled photon excited fluorescence in organic materials: an ultrafast coincidence detector. *J. Phys. Chem. Lett.* **2017**, *8*, 388−393.
(26) Raymer, M. G.; Marcus, A. H.; Widom, J. R.; Vitullo, D. L. Entangled photon-pair two-dimensional fluorescence spectroscopy (EPP-2DFS). *J. Phys. Chem. B* **2013**, *117*, 15559−15575.
(27) Ye, L.; Mukamel, S. Interferometric two-photon-absorption spectroscopy with three entangled photons. *Appl. Phys. Lett.* **2020**, *116*, 174003.
(28) Villabona-Monsalve, J. P.; Varnavski, O.; Palfey, B. A.; Goodson, T. Two-Photon Excitation of Flavins and Flavoproteins with Classical and Quantum Light. *J. Am. Chem. Soc.* **2018**, *140*, 14562−14566.
(29) Raymer, M. G.; Landes, T.; Marcus, A. H. Entangled Two-Photon Absorption by Atoms and Molecules: A Quantum Optics Tutorial. *arXiv:2103.02551* **2021**, na.
(30) Gu, B.; Mukamel, S. Manipulating Two-Photon-Absorption of Cavity Polaritons by Entangled Light. *J. Phys. Chem. Lett.* **2020**, *11*, 8177−8182.
(31) Kelley, A. M. Hyper-Raman Scattering by Molecular Vibrations. *Annu. Rev. Phys. Chem.* **2010**, *61*, 41−61.
(32) Christie, J. H.; Lockwood, D. J. Selection Rules for Three- and Four-Photon Raman Interactions. *J. Chem. Phys.* **1971**, *54*, 1141−1154.
(33) Shoute, L. C.; Bartholomew, G. P.; Bazan, G. C.; Kelley, A. M. Resonance hyper-Raman excitation profiles of a donor-acceptor substituted distyrylbenzene: One-photon and two-photon states. *J. Chem. Phys.* **2005**, *122*, 184508.
(34) Shoute, L. C.; Blanchard-Desce, M.; Kelley, A. M. Resonance Hyper-Raman Excitation Profiles and Two-Photon States of a Donor-Acceptor Substituted Polyene. *J. Phys. Chem. A* **2005**, *109*, 10503−10511.
(35) Myers Kelley, A. Resonance Raman and resonance hyper-Raman intensities: structure and dynamics of molecular excited states in solution. *J. Phys. Chem. A* **2008**, *112*, 11975−11991.
(36) Leng, W.; Kelley, A. M. Hyper-Rayleigh and hyper-Raman scatterings with intermediate and two-photon resonances. *J. Chem. Phys.* **2007**, *127*, 164509.
(37) Loudon, R. *The Quantum Theory of Light*; Oxford University Press, 2000; Chapter 9.
(38) Mukamel, S. *Principles of Nonlinear Optical Spectroscopy*; Oxford University Press, 1995; Chapter 6.

https://doi.org/10.1021/acsphotonics.1c00777
ACS Photonics XXXX, XXX, XXX−XXX

SI: Vibrational Hyper-Raman Molecular Spectroscopy with Entangled Photons

Feng Chen and Shaul Mukamel*

Department of Chemistry and Department of Physics & Astronomy, University of California, Irvine, CA 92697, USA

E-mail: smukamel@uci.edu

S1 The expressions for S_{II} and S_{III} with entangled photons

$$
\begin{aligned}
S_{II}(\omega_r) = {} & \frac{\pi|\alpha_P|^2}{T_e} L(\bar{\omega}_i)^2 L(\bar{\omega}_s)^2 \sum_{g',e,e',f,f'} \sum_{\boldsymbol{p}} \frac{V_{ge'} V_{e'f'} V^*_{g'f'} V_{g'f} V^*_{ef} V^*_{ge}}{(\omega_{f'g'} - \omega_r + i\gamma_{f'g'})(\bar{\omega}_{\boldsymbol{p}_1} - \omega_{eg} + i\gamma_{eg})} \\
& \times \Bigg\{ \frac{1}{\bar{\omega}_{\boldsymbol{p}_4} - \omega_{fe'} + i\gamma_{fe'}} \frac{e^{i(\bar{\omega}_{\boldsymbol{p}_4} + \omega_{e'g'} - \omega_r + i\gamma_{e'g'})T_e/2} - 1}{i(\bar{\omega}_{\boldsymbol{p}_4} + \omega_{e'g'} - \omega_r + i\gamma_{e'g'})} \left[\frac{1}{\omega_{e'e} + \bar{\omega}_{\boldsymbol{p}_1} - \bar{\omega}_{\boldsymbol{p}_3} + i\gamma_{e'e}} - \frac{e^{i(\bar{\omega}_{\boldsymbol{p}_1} - \omega_{eg} + i\gamma_{eg})T_e/2}}{\omega_{e'g} - \bar{\omega}_{\boldsymbol{p}_3} + i\gamma_{e'e} - i\gamma_{eg}} \right] \\
& + \frac{e^{i(\bar{\omega}_{\boldsymbol{p}_4} - \omega_{fe'} + i\gamma_{fe'})T_e/2}}{\omega_{fe'} - \bar{\omega}_{\boldsymbol{p}_4} - i\gamma_{fe'}} \frac{e^{i(\omega_{fg'} - \omega_r + i\gamma_{e'g'} - i\gamma_{fe'})T_e/2} - 1}{i(\omega_{fg'} - \omega_r + i\gamma_{e'g'} - i\gamma_{fe'})} \left[\frac{1}{\omega_{e'e} + \bar{\omega}_{\boldsymbol{p}_1} - \bar{\omega}_{\boldsymbol{p}_3} + i\gamma_{e'e}} - \frac{e^{i(\bar{\omega}_{\boldsymbol{p}_1} - \omega_{eg} + i\gamma_{eg})T_e/2}}{\omega_{e'g} - \bar{\omega}_{\boldsymbol{p}_3} + i\gamma_{e'e} - i\gamma_{eg}} \right] \\
& + \frac{e^{i(\omega_{e'e} + \bar{\omega}_{\boldsymbol{p}_1} + \bar{\omega}_{\boldsymbol{p}_4} - \omega_{fg} + i\gamma_{fe'} + i\gamma_{eg})T_e/2}}{(\bar{\omega}_{\boldsymbol{p}_3} - \omega_{e'g} - i\gamma_{e'e} + i\gamma_{eg})(\omega_P - \omega_{fg} + i\gamma_{fe'} + i\gamma_{eg} - i\gamma_{e'e})} \frac{e^{i(\omega_{fg'} - \omega_r + i\gamma_{e'g'} - i\gamma_{fe'})T_e/2} - 1}{i(\omega_{fg'} - \omega_r + i\gamma_{e'g'} - i\gamma_{fe'})} \\
& + \frac{e^{i(\omega_{e'e} + \bar{\omega}_{\boldsymbol{p}_1} - \bar{\omega}_{\boldsymbol{p}_3} + i\gamma_{e'e})T_e/2}}{(\omega_{e'g} - \bar{\omega}_{\boldsymbol{p}_3} + i\gamma_{e'e} - i\gamma_{eg})(\omega_P - \omega_{fg} + i\gamma_{fe'} + i\gamma_{eg} - i\gamma_{e'e})} \frac{e^{i(\omega_P - \omega_r - \omega_{g'g} + i\gamma_{e'g'} + i\gamma_{eg} - i\gamma_{e'e})T_e/2} - 1}{i(\omega_P - \omega_r - \omega_{g'g} + i\gamma_{e'g'} + i\gamma_{eg} - i\gamma_{e'e})} \\
& + \frac{e^{i(\bar{\omega}_{\boldsymbol{p}_4} - \omega_{fe'} + i\gamma_{fe'})T_e/2}}{(\omega_{e'e} + \bar{\omega}_{\boldsymbol{p}_1} - \bar{\omega}_{\boldsymbol{p}_3} + i\gamma_{e'e})(\bar{\omega}_{\boldsymbol{p}_2} - \omega_{fe} + i\gamma_{fe} - i\gamma_{e'e})} \frac{e^{i(\omega_{fg'} - \omega_r + i\gamma_{e'g'} - i\gamma_{fe'})T_e/2} - 1}{i(\omega_{fg'} - \omega_r + i\gamma_{e'g'} - i\gamma_{fe'})} \\
& - \frac{e^{i(\omega_{e'e} + \bar{\omega}_{\boldsymbol{p}_1} - \bar{\omega}_{\boldsymbol{p}_3} + i\gamma_{e'e})T_e/2}}{(\omega_{e'e} + \bar{\omega}_{\boldsymbol{p}_1} - \bar{\omega}_{\boldsymbol{p}_3} + i\gamma_{e'e})(\bar{\omega}_{\boldsymbol{p}_2} - \omega_{fe} + i\gamma_{fe'} - i\gamma_{e'e})} \frac{e^{i(\bar{\omega}_{\boldsymbol{p}_2} + \omega_{eg'} - \omega_r + i\gamma_{e'g'} - i\gamma_{e'e})T_e/2} - 1}{i(\bar{\omega}_{\boldsymbol{p}_2} + \omega_{eg'} - \omega_r + i\gamma_{e'g'} - i\gamma_{e'e})} \Bigg\}
\end{aligned}
\tag{S1}
$$

and

$$
\begin{aligned}
S_{III}(\omega_r) = \frac{\pi|\alpha_P|^2}{T_e} L(\bar{\omega}_i)^2 L(\bar{\omega}_s)^2 \sum_{g',e,e',f,f'} \sum_{\boldsymbol{p}} \frac{V_{ge'} V_{e'f'} V^*_{g'f'} V_{g'f} V^*_{ef} V^*_{ge}}{(\omega_{f'g'} - \omega_r + i\gamma_{f'g'})(\omega_{e'g} - \bar{\omega}_{\boldsymbol{p}_3} + i\gamma_{e'g})} \\
\times \Bigg\{ \frac{1}{(\bar{\omega}_{\boldsymbol{p}_4} - \omega_{fe'} + i\gamma_{fe'})(\omega_{e'e} + \bar{\omega}_{\boldsymbol{p}_1} - \bar{\omega}_{\boldsymbol{p}_3} + i\gamma_{e'e})} \frac{e^{i(\bar{\omega}_{\boldsymbol{p}_4} + \omega_{e'g'} - \omega_r + i\gamma_{e'g'})T_e/2} - 1}{i(\bar{\omega}_{\boldsymbol{p}_4} + \omega_{e'g'} - \omega_r + i\gamma_{e'g'})} \\
- \frac{e^{i(\bar{\omega}_{\boldsymbol{p}_4} - \omega_{fe'} + i\gamma_{fe'})T_e/2}}{(\bar{\omega}_{\boldsymbol{p}_4} - \omega_{fe'} + i\gamma_{fe'})(\omega_{e'e} + \bar{\omega}_{\boldsymbol{p}_1} - \bar{\omega}_{\boldsymbol{p}_3} + i\gamma_{e'e})} \frac{e^{i(\omega_{fg'} - \omega_r + i\gamma_{e'g'} - i\gamma_{fe'})T_e/2} - 1}{i(\omega_{fg'} - \omega_r + i\gamma_{e'g'} - i\gamma_{fe'})} \\
- \frac{e^{i(\omega_{e'g} - \bar{\omega}_{\boldsymbol{p}_3} + i\gamma_{e'g})T_e/2}}{(\bar{\omega}_{\boldsymbol{p}_1} - \omega_{eg} + i\gamma_{e'e} - i\gamma_{e'g})(\omega_P - \omega_{fg} + i\gamma_{fe'} - i\gamma_{e'g})} \frac{e^{i(\omega_P - \omega_r - \omega_{g'g})T_e/2} - 1}{i(\omega_P - \omega_r - \omega_{g'g})} \\
+ \frac{e^{i(\bar{\omega}_{\boldsymbol{p}_4} - \omega_{fe'} + i\gamma_{fe'})T_e/2}}{(\bar{\omega}_{\boldsymbol{p}_1} - \omega_{eg} + i\gamma_{e'e} - i\gamma_{e'g})(\omega_P - \omega_{fg} + i\gamma_{fe'} - i\gamma_{e'g})} \frac{e^{i(\omega_{fg'} - \omega_r + i\gamma_{e'g} - i\gamma_{fe'})T_e/2} - 1}{i(\omega_{fg'} - \omega_r + i\gamma_{e'g} - i\gamma_{fe'})} \\
+ \frac{e^{i(\omega_{e'e} + \bar{\omega}_{\boldsymbol{p}_1} - \bar{\omega}_{\boldsymbol{p}_3} + i\gamma_{e'e})T_e/2}}{(\bar{\omega}_{\boldsymbol{p}_1} - \omega_{eg} + i\gamma_{e'e} - i\gamma_{e'g})(\bar{\omega}_{\boldsymbol{p}_2} - \omega_{fe} + i\gamma_{fe'} - i\gamma_{e'e})} \frac{e^{i(\bar{\omega}_{\boldsymbol{p}_2} + \omega_{eg'} - \omega_r + i\gamma_{e'g'} - i\gamma_{e'e})T_e/2} - 1}{i(\bar{\omega}_{\boldsymbol{p}_2} + \omega_{eg'} - \omega_r + i\gamma_{e'g'} - i\gamma_{e'e})} \\
- \frac{e^{i(\bar{\omega}_{\boldsymbol{p}_4} - \omega_{fe'} + i\gamma_{fe'})T_e/2}}{(\bar{\omega}_{\boldsymbol{p}_1} - \omega_{eg} + i\gamma_{e'e} - i\gamma_{e'g})(\bar{\omega}_{\boldsymbol{p}_2} - \omega_{fe} + i\gamma_{fe'} - i\gamma_{e'e})} \frac{e^{i(\omega_{fg'} - \omega_r + i\gamma_{e'g'} - i\gamma_{fe'})T_e/2} - 1}{i(\omega_{fg'} - \omega_r + i\gamma_{e'g'} - i\gamma_{fe'})} \\
- \frac{e^{i(\omega_{e'e} + \bar{\omega}_{\boldsymbol{p}_1} - \bar{\omega}_{\boldsymbol{p}_3} + i\gamma_{e'e})T_e/2}}{(\omega_{e'e} + \bar{\omega}_{\boldsymbol{p}_1} - \bar{\omega}_{\boldsymbol{p}_3} + i\gamma_{e'e})(\bar{\omega}_{\boldsymbol{p}_2} - \omega_{fe} + i\gamma_{fe'} - i\gamma_{e'e})} \frac{e^{i(\bar{\omega}_{\boldsymbol{p}_2} + \omega_{eg'} - \omega_r + i\gamma_{e'g'} - i\gamma_{e'e})T_e/2} - 1}{i(\bar{\omega}_{\boldsymbol{p}_2} + \omega_{eg'} - \omega_r + i\gamma_{e'g'} - i\gamma_{e'e})} \\
+ \frac{e^{i(\bar{\omega}_{\boldsymbol{p}_4} - \omega_{fe'} + i\gamma_{fe'})T_e/2}}{(\omega_{e'e} + \bar{\omega}_{\boldsymbol{p}_1} - \bar{\omega}_{\boldsymbol{p}_3} + i\gamma_{e'e})(\bar{\omega}_{\boldsymbol{p}_2} - \omega_{fe} + i\gamma_{fe'} - i\gamma_{e'e})} \frac{e^{i(\omega_{fg'} - \omega_r + i\gamma_{e'g'} - i\gamma_{fe'})T_e/2} - 1}{i(\omega_{fg'} - \omega_r + i\gamma_{e'g'} - i\gamma_{fe'})} \Bigg\}
\end{aligned}
\tag{S2}
$$

S2 Hyper-Raman and fluorescence signals for the one-photon off-resonant but two-photon resonant experimental setting

In the main text, we have focused on the experimental setting with one-photon resonances but no two-photon resonance to avoid two-photon induced fluorescence. For completeness, here we investigate the more common experimental setting with two-photon resonances but no one-photon resonance, and study whether the entanglement has effects on the signals.

The signal has two contributions: hyper-Raman scattering and two-photon induced fluorescence. The former is described by the diagram (A) in Fig. S1 and its conjugate, but the

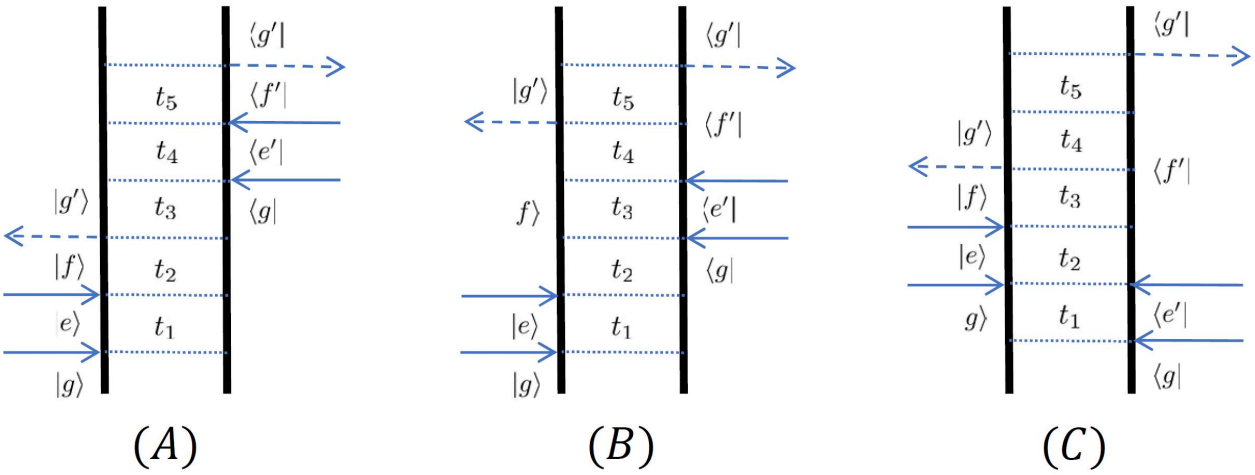

Figure S1: Ladder diagrams representing the Liouville-space pathways of HR and fluorescence signals for systems with two-photon resonant doubly-excited states but one-photon off-resonant intermediate states. Their complex conjugates are given by other diagrams(not shown). Diagram (A) corresponds to hyper-Raman scattering whereas (B) and (C) correspond to two-photon induced fluorescence.

latter by diagram (B-C) and their conjugates.

In Fig. S2, we show separately the total signals produced by a classical monochromatic pulse and degenerate entangled photons. One note that in both plots, the narrow HR signals are much weaker than the fluorescence, which can erode the signal-to-noise ratio of the HR spectrum. However, fluorescence is avoided in the one-photon resonant but two-photon off-resonant setting introduced in the main text.

We find that photon entanglement has no effect on the relative intensities of fluorescence and Hyper-Raman scattering. That is expected because entanglement only imposes a correlation between the arrival times of first two photons, whereas it puts no restriction on the time interval between two-photon absorption and the last photon emission. In fact, even with classical light, two photons are almost absorbed simultaneously when there is no one-photon resonance because of the Heisenberg uncertainty relation. Therefore, the time correlation of the entangled photons has little effect on the signals. The major difference between the classical and quantum signals is their quadratic vs linear scaling with the pump intensity, but this scaling is the same for the fluorescence and Raman components and therefore will

enhance both equally at low pump intensities without changing their relative magnitudes. This is confirmed in Fig. S2(b), where both components are enhanced by $\frac{\pi|\alpha_P|^2}{T_e}/|\alpha_P|^4 \approx 300$ times.

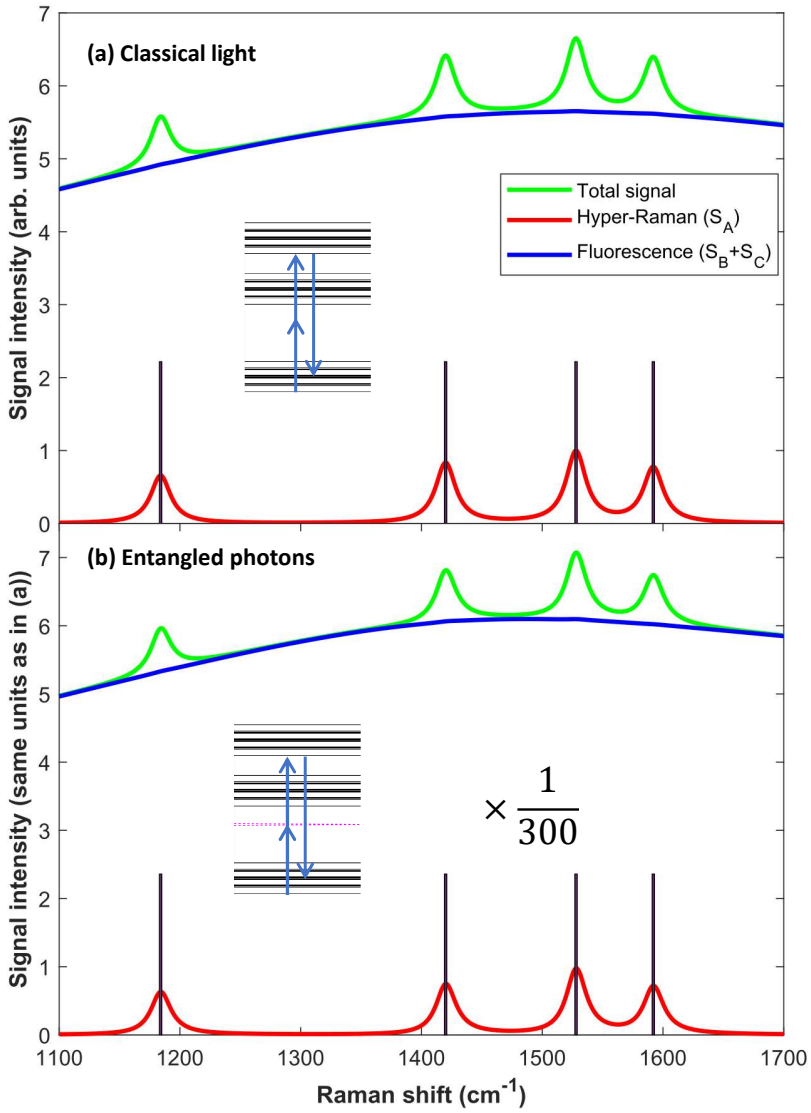

Figure S2: HR scattering and two-photon induced fluorescence: classical light vs. entangled photons. (a) Classical monochromatic pulse: $\omega_c = 12900$ cm^{-1}; (b) Degenerate entangled photons: $\omega_i = \omega_s = 12900$ cm^{-1} and $T_e = 1$ps. Fluorescence dominates over HR scattering and the photon entanglement has no effects on their relative intensities but simply enhance them equally at a low pump intensity. Other parameters are the same as in Fig. 3.